Fast diagnostics of BRAF mutations in biopsies from malignant melanoma

François Huber*,†, Hans Peter Lang†, Katharina Glatz‡, Donata Rimoldi§, Ernst Meyer†,

Christoph Gerber*,†

† Swiss Nanoscience Institute, Department of Physics, University of Basel, CH-4056 Basel, Switzerland

‡ Institute of Pathology, University Hospital Basel, CH-4031 Basel, Switzerland

§ Ludwig Center for Cancer Research, University of Lausanne, CH-1066 Epalinges, Switzerland

ABSTRACT: According to the American skin cancer foundation, there are more new cases of skin cancer than the combined incidence of cancers of the breast, prostate, lung and colon each year and malignant melanoma represents its deadliest form. About 50% of all cases are characterized by a particular mutation $BRAF^{V600E}$ in the $BRAF$-gene. Recently developed highly specific drugs are able to fight $BRAF^{V600E}$ mutated tumors, but require diagnostic tools for fast and reliable mutation detection to warrant treatment efficiency. We completed a preliminary clinical trial applying cantilever array sensors to demonstrate identification of a $BRAF^{V600E}$ single-point mutation using total RNA obtained from biopsies of metastatic melanoma of diverse

1

sources (surgical material either frozen or fixated with formalin and embedded in paraffin). The method is faster than the standard Sanger or pyrosequencing methods and comparably sensitive as next-generation sequencing. Processing time from biopsy to diagnosis is below one day and does not require PCR-amplification, sequencing and labels.

Cancer is the number one cause of death worldwide surpassing cardiovascular disease or all strokes[1]. The most common malignancy in humans is skin cancer[2]. The occurrence of cutaneous malignant melanoma has steadily increased over the past 50 years in fair-skinned populations and still grows in many developed countries as a result of changing sun-seeking behavior. Only up to 5% of all skin cancers are malignant melanomas, but are responsible for almost all fatalities. However, recently novel treatment methods have been developed. They are based on compounds with high specificity that have initiated stratified healthcare therapies by targeting particular driver mutations in various genes, e.g. BRAF inhibitors like vemurafenib for patients with $BRAF^{V600E}$ mutated tumors[3,4]. In combination with new mitogen-activated protein kinase kinase (MAP2K, MEK, MAPKK) inhibitors such as cobimetinib[5] life expectancy can be extended to about one year[6] with fewer side effects than the standard chemotherapeutic drug dacarbazine. The current gold standard for mutation screening in malignant tumors uses real-time polymerase chain reaction (PCR) and sequencing methods for DNA extracted from biopsies. Our method neither needs PCR, nor labelling, nor sequencing. PCR protocols can be error-prone with false positives as a particular hazard. Artifacts complicate protocols[7] and extend processing time. We use an array of nanomechanical microcantilevers for surface stress sensing based on atomic force microscopy[8] to analyze DNA/DNA hybridization[9-12]. The technique was further adapted to reveal antigen/antibody[13,14], transcription factor/DNA interactions[15] and effects of antibiotics on bacteria[16]. The platform also proved applicability to study transcriptional

2

activity of genes[17,18] and is able to characterize function of transmembrane protein activity[19]. Here, we report on the detection of the *BRAF^V600E* mutation present in a subset of 50-60% malignant melanomas in human biopsies at the RNA level. We chose to use RNA since more RNA transcripts occur in the cytoplasm than genomic DNA counterparts. Moreover, RNA/DNA heterodimers have a higher thermodynamic stability than DNA/DNA homodimers. The hybrid double helix shows an increased hydrodynamic radius (DNA/DNA 1.07 ±0.03 nm vs. RNA/DNA 1.27 ±0.03 nm)[20], which should result in a higher stress on the cantilever's surface due to steric hindrance, thereby increasing the sensitivity of the technique. Different oligonucleotides were designed to uniquely recognize the altered BRAF sequence. Searching the human genome expressed sequence tags database[21] an 18 base sequence was chosen to detect unambiguously the BRAF mRNA transcript. Our array sensor device facilitates addressing other mutations such as *BRAF^V600K* for a more thorough investigation of tumors.

The working principle of nanomechanical microcantilever biosensors is depicted in a schematic way in Figure 1a and in an experimental setup in supporting information, Figure S1. A self-assembled monolayer (SAM) of thiol-modified probe oligonucleotides (Supporting information Table S1) is covalently bound to gold-coated surfaces of the cantilevers. Upon hybridization with target oligonucleotides, bending of cantilevers is observed due to steric and ionic repulsion forces. Initial experiments to determine optimized hybridization conditions were performed (Supporting information Figure S2) in order to estimate the lowest ratio of mutant to wild type BRAF RNA (Figure 1b) required to conclusively identify the mutation by measuring various ratios.

3
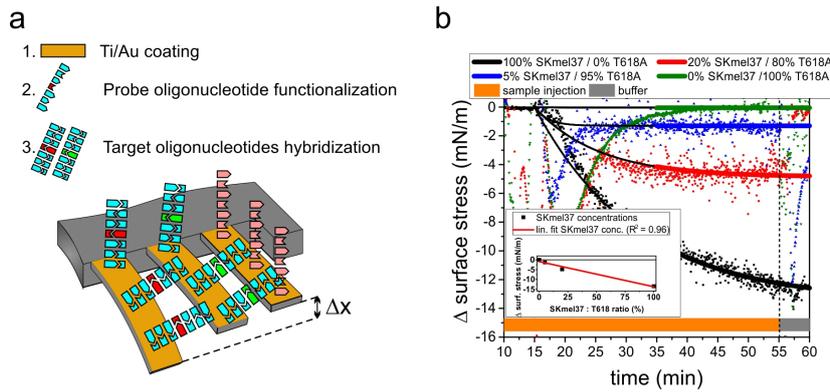
Figure 1. Schematic of a cantilever array demonstrating surface modifications for the detection of BRAF RNA. (a) Steps: 1. coating 8 cantilevers with Ti (adhesion layer) and Au for functionalization with thiols; 2. adsorption of oligonucleotides for mutation recognition (site of mutation shown in red), wild type detection as a control (wild type site in green) or as non-specific reference (polyAC; pink); 3. Experiment: total RNA injection containing complementary target sequences. Light blue indicates non-related sequences. The probe cantilevers will bend on hybridization depending on the presence of the mutation or the wild type or both, yielding a differential deflection Δx. All measurements must be done in a differential way to get reliable results, allowing to exclude undesired influences from temperature and non-specific adsorption. (b) Assessing the minimum RNA concentration for $BRAF^{V600E}$ detection using samples from cell lines: Various ratios of SK-Mel-37 $BRAF^{V600E}$ positive to T618A $BRAF^{V600E}$ negative total RNA (0%, 5%, 20% and 100%) have been used. We superimposed Langmuir isotherms ($R^2 > 0.94$) on top of the data including the first 20 minutes dominated by mixing effects. The inset shows that the extrapolated differential deflections scale with the SK-Mel-37 concentrations.

4

The following two melanoma cell lines were selected (Ludwig Institute for Cancer Research, Univ. Lausanne): T618A carrying wild type *BRAF* and SK-Mel-37 carrying *BRAF^{V600E}*. The T618A line expresses a wild type form of BRAF, whereas the SK-Mel-37 line expresses the *BRAF^{V600E}* mutant, and - to a lower extent - the wild type allele. Samples of total RNA obtained from two melanoma cell lines were mixed at different ratios and injected into the measurement chamber at a concentration of 20 ng/μl. The lowest ratio of 5% mutant in total wild type RNA turned out to be sufficient to identify the mutation in total RNA extracted from cell lines. A fraction of 5% is comparable to the amount other current methods require such as the COBAS test[22] and represents a 4-fold improvement over standard PCR/sequencing.

Having established the conditions for *BRAF^{V600E}* detection in different cell lines, the next step is to extend the investigation to biopsies of melanoma patients by performing a clinical pilot study comprising 9 patients (Pathology Department of the University Hospital Basel). Two representative measurements are shown from *BRAF^{V600E}* positive (Figure 2a) and from *BRAF^{V600E}* negative (Figure 2b) melanoma biopsies. Melanoma tumors can be very heterogeneous with respect to their tumor cell expression profiles[23] and may contain variable levels of normal cells (Table 1). We obtained a large signal of -15 mN/m (red curve) in a *BRAF^{V600E}* positive tumor biopsy (Figure 2a) in contrast to a small signal of +3.0 mN/m in a *BRAF^{V600E}* negative tumor biopsy (Figure 2b). A large response (red curve) of the *BRAF^{V600E}* detecting cantilever is a clear indicator for the presence of the *BRAF^{V600E}* mutation, whereas the green curve does not interrogate *BRAF^{V600E}*. We observed a substantial signal of -25mN/m for wild type *BRAF* (green curve) as the *BRAF^{V600E}* positive melanoma also expresses the wild type allele to a large extent. Therefore, the presence of *BRAF^{V600E}* is unambiguously verified in the *BRAF^{V600E}* positive tumor biopsy sample. We performed 9 analyses on human malignant melanoma biopsies (Biopsy_1 -

5

Biopsy_9), as well as 21 analyses on tissue cultures (TC) *BRAF*[V600E] positive (10 samples, labelled TC_1 – TC_10) and negative cell lines (11 samples, labelled TC_11 – TC_21). Samples originated from formaldehyde-fixed, paraffin-embedded, FFPE, and frozen tissues.
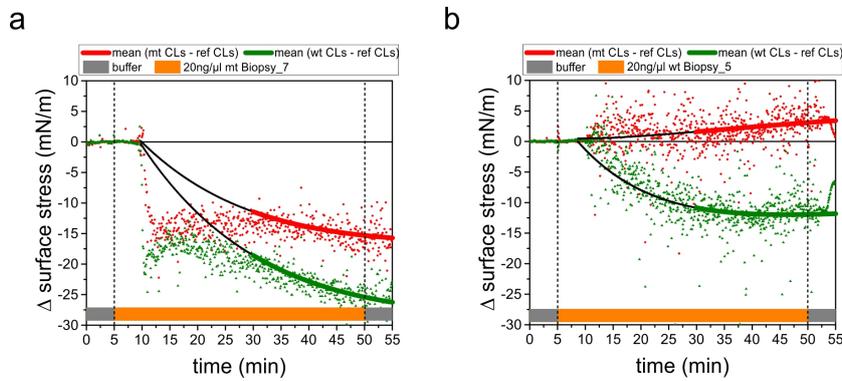
Figure 2. RNA samples from two biopsies are investigated. The red curve represents the difference of responses between mutant probe (mt) and polyAC reference cantilever (ref) implying presence of *BRAF*[V600E]. The green curve shows a combination of wt reference and polyAC reference cantilevers indicating wild type *BRAF*. (a) *BRAF*[V600E] positive Biopsy_7 exhibiting a non zero signal (red curve). (b) *BRAF*[V600E] negative Biopsy_5 showing a signal around zero in the red curve (for biopsy numbers and origin see Table 1). Langmuir fits ($R^2 >$ 0.95) are superimposed on top of the data.

6

Table 1. Clinical sample analysis.

Number	Type of Biopsy	Origin	RNA yield. (µg)	RNA conc. (ng/µl)	BRAF Status Pathology	BRAF Evaluation Cantilever	% tumor cells as determined in pathology
Biopsy_1	FFPE	Lung metastasis	9.4	188	Mutant	**Mutant**	95%
Biopsy_2	Frozen	Mesenteric metastasis	48.45	969	Wild Type	**Wild Type**	90%
Biopsy_3	FFPE	Mesenteric metastasis	78.15	1563	Wild Type	**Wild Type**	not done
Biopsy_4	Frozen	Axillary lymph node metastasis	11.7	234	Wild Type	**Wild Type**	whole slide: 50%; marked area: 95%
Biopsy_5	FFPE	Axillary lymph node metastasis	417	8340	Wild Type	**Wild Type**	not done
Biopsy_6	FFPE	Cutaneous metastasis	626.95	12539	Mutant	**Mutant**	whole slide: 95%; marked area: 98%
Biopsy_7	FFPE	Lymph node metastasis	94.2	1885	Mutant	**Mutant**	marked area: 98%
Biopsy_8	FFPE	Axillary lymph node metastasis	133.2	2666	Wild Type	**Wild Type**	marked area: 98%
Biopsy_9	FFPE	Pleural metastasis	39.5	792	Mutant	**Mutant**	marked area: 98%

Total RNA was extracted from formalin-fixed paraffin-embedded tissue (FFPE) or frozen tumor samples. The RNA yield as well as the percentage of tumor cells estimated by a pathologist and total RNA concentrations of each biopsy are displayed. Three biopsies were additionally characterized by next generation sequencing (Biopsy_2, Biopsy_4, and Biopsy_8).

We processed the data in a hierarchical cluster analysis (Figure 3 and Methods in supporting information) and were able to distinguish results obtained on cell lines and clinical samples (with the mutation in red and without the mutation in green). The dendrogram (tree structure) calculated using the method of Euclidian distances shows a bifurcation that reveals two main clusters representing mutant and wild type samples in both cell lines and clinical samples. The $BRAF^{V600E}$ positive biopsies are clearly part of the mutation cluster and the $BRAF^{V600E}$ negative biopsies are part of the wild type cluster, manifesting the single point mutation sensitivity of our method. The fact that $BRAF^{V600E}$ biopsies and the different preparations of tissue culture samples bifurcate earlier (*) than the wild type biopsies and the corresponding tissue culture preparations do (**), reflects a higher variability in the biopsies. The $BRAF^{V600E}$ positive biopsies are part of two different branches of the bifurcation (*). Biopsy_1 and Biopsy_7 are part of one branch,

whereas Biopsy_6 and Biopsy_9 are members of the second branch. In contrast, the majority of the wild type biopsies including Biopsy_3, 8, 4, 5 belong to the same branch of bifurcation (**), and only Biopsy_2 is member of the other branch. These findings point towards a genetically more heterogeneous nature of the *BRAF*[V600E] biopsies and tissue culture samples as compared to the BRAF wild type biopsies and tissue cultures. A probable explanation is that different expression levels in the various samples influence the differential deflection signals. For comparison of our observations with the histological and sequencing findings we compiled Table 1 showing the state, origin and type of biopsies. Our results agree with those obtained with standard methods of amplification and sequencing. In addition, our method provides high sensitivity requiring only 5% of cancer cells in the sample containing the *BRAF*[V600E] mutation and is comparable to the most sensitive sequencing methods currently in use.
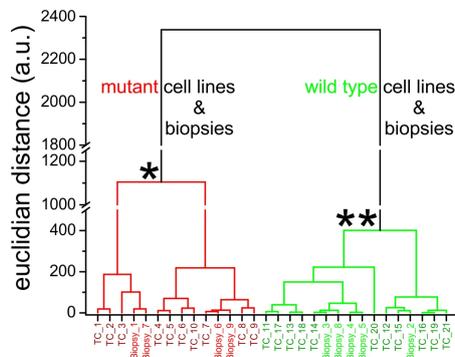
Figure 3. Hierarchical cluster analysis including 10 *BRAF*[V600E] positive tissue culture samples (TC_1 –TC_10, red), 11 *BRAF*[V600E] negative tissue culture samples (TC_11 – TC_21, green) and 9 biopsies (Biopsy_1 – Biopsy_9). The *BRAF*[V600E] positive biopsies 1, 6, 7, and 9 (red) are clearly distinguished from the *BRAF*[V600E] negative 2, 3, 4, 5, and 8 biopsies (green).

Our method is capable of a more detailed mutation analysis. $BRAF^{V600K}$ is another less frequent mutation present in 10% of incidences. BRAFV600K oligonucleotide targets allow to distinguish the $BRAF^{V600E}$ and $BRAF^{V600K}$ mutations. Exposing the corresponding cantilevers to BRAFV600K complements results in bending (Figure 4a), whereas the BRAFV600E cantilevers respond in the corresponding experiment with BRAFV600E complement (Figure 4b), emphasizing mutation discrimination. These experiments support the specificity of the assay and show the versatility of the cantilever array in investigating relevant multiple mutations simultaneously. The method does neither require PCR sample amplification nor labelling due to the fact that total RNA is used. Faster recognition of multiple mutations is achived using parallel measurements owing to microcantilever arrays.
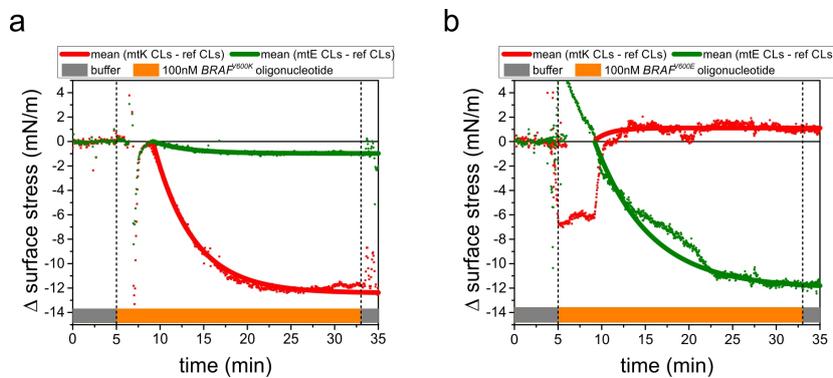
Figure 4. Analysis of $BRAF^{V600K}$ mutation using BRAFV600K and BRAFV600E complement oligonucleotides. Microcantilevers were functionalized with BRAFV600K, BRAFV600E and polyAC oligonucleotide. Shown in red: response difference between mutant BRAFV600K and polyAC reference. Shown in green: response difference between mutant BRAFV600E and polyAC reference. Smooth lines represent Langmuir fits ($R^2 > 0.95$). (a) injection of 100 nM BRAFV600K complement and (b) 100 nM BRAFV600E complement.

The proposed method has the following advantages: 1. neither PCR sample amplification nor labelling is necessary due to the fact that total RNA is employed; 2. the technique avoids costly sample preparation steps and 3. the array format allows parallel simultaneous interrogation of multiple targetable mutations for an efficient analysis in one assay; 4. both fresh and routine paraffin embedded tissue (a single 20 μm thick slice) may be used; 5. high sensitivity equivalent to the current sequencing technologies.

Here, the aim was to study *BRAF* mutations in melanoma. However, nanomechanical cantilevers may also be used for the detection of any point mutation, like BRCA1 and BRCA2 gene mutations in breast cancer. Another important breast cancer marker that is used to make treatment decisions is HER2. The HER2 gene is amplified which results in multiple copies of the gene as well as in increased expression of the HER2 protein. In a preliminary study, we already detected the amplified gene using specific oligonucleotide probes to demonstrate the versatility of our method. Moreover, protein overexpression is likely to be assessed using specific antibodies, reducing two different detection methods into one single microcantilever based assay. Gene mutation and protein expression analysis is also applicable to CRISPR/CAS9 gene editing, as insertions and deletions down to single point mutations can be easily verified, underlining the potential of the microcantilever technology.

ASSOCIATED CONTENT

Supporting Information.

Methods, table S1, and figures (Figures S1 and S2).

10

This material is available free of charge via the Internet at http://pubs.acs.org.

AUTHOR INFORMATION

Corresponding Author

*E_mail: francois.huber@unibas.ch.

*E_mail: christoph.gerber@unibas.ch.

Author Contributions

The study was conceived by F.H., H.P.L., K.G. and C.G. The experiments were designed and interpreted by F.H. and K.G. The experiments were performed and analyzed by F.H. DNA/RNA samples were prepared by K.G. and D.R. Cantilever arrays were prepared by H.P.L. and F.H. The manuscript was written by F.H., K.G., H.P.L., C.G. and E.M. All authors participated in the discussion of results and contributed valuable comments.

Notes

The authors declare that they have no competing financial interests.

Formatted: German (Switzerland)

11

ABBREVIATIONS

BRAF Rapid Acceleration of Fibrosarcoma gene B

REFERENCES

1. Ferlay, J.; Soerjomataram, I.; Dikshit, R.; Eser, S.; Mathers, C.; Rebelo, M.; Parkin, D. M.; Forman, D.; Bray, F. *Int. J. Cancer* **2015***, 136*, E359–E386.

2. Simões, M.C.F.; Sousa, J.J.S.; Pais, A.A.C.C. *Cancer Lett*. **2015**, *357*, 8-42.

3. Ravnan, M.C.; Matalka, M.S. *Clin. Ther*. **2012**, *34*, 1474-1486.

4. Akbani, R.; Akdemir, K. C.; Aksoy, B. A.; Albert, M.; Ally, A.; Amin, S. B.; Arachchi, H.; Arora, A.; J. Auman, J. T.; Ayala, B.; et al. *Cell* **2015***, 161*, 1681–1696.

5. Hatzivassiliou, G.; Haling, J. R.; Chen, H.; Song, K.; Price, S.; Heald, R.; Hewitt, J. F. M.; Zak, M.; Peck, A.; Orr, C.; et al. *Nature* **2013**, *501*, 232–236.

12

6. Larkin, J. M. G.; Yan, Y. B.; McArthur, G. A.; Ascierto, P. A.; Liszkay, G.; Maio, M.; Mandala, M.; Demidov, L. V.; Stroyakovskiy, D.; Thomas, L.; et al. *J. Clin. Oncol.* **2015**, *33* (suppl. S) Abstract: 9006.

7. Lenz, T.L.; Becker, S. *Gene* **2013**, *427*, 117-123.

8. Binnig, G.; Quate, C.F.; Gerber, C. *Phys. Rev. Lett.* **1986**, *56*, 930-933.

9. Fritz, J.; Baller, M. K.; Lang, H. P.; Rothuizen, H.; Vettiger, P.; Meyer, E.; Güntherodt, H.-J.; Gerber, C.; Gimzewski, J. K. *Science* **2000**, *288*, 316-318.

10. Hansen, K.M.; Ji, H.-F.; Wu, G.; Ram Datar, R.; Cote, R.; Majumdar, A.; Thundat T. *Anal. Chem.* **2001**, *73*, 1567-1571.

11. McKendry, R.; Zhang, J.; Arntz, Y.; Strunz, T.; Hegner, M.; Lang, H. P.; Baller, M. K.; Certa, U.; Meyer, E.; Güntherodt, H.-J.; Gerber C. *Proc. Natl. Acad. Sci. U.S.A.* **2001**, *99*, 9783-9788.

12. Alvarez, M.; Carrascosa, L. G.; Moreno, M.; Calle, A.; Zaballos, Á.; Lechuga, L. M.; Martínez-A, C.; Tamayo, J. *Langmuir* **2004**, *20*, 9663-9668.

13. Arntz, Y.; Seelig, J. D.; Lang, H. P.; Zhang, J.; Hunziker, P.; Ramseyer, J. P.; Meyer, E.; Hegner, M.; Gerber, C. *Nanotechnology* **2002,** *14*, 86-90.

14. Backmann, N.; Zahnd, C.; Huber, F.; Bietsch, A.; Plückthun, A.; Lang, H. P.; Güntherodt, H.-J.; Hegner, M.; Gerber, C. *Proc. Natl. Acad. Sci. U.S.A.* **2005,** *102*, 14587-14592.

15. Huber, F.; Hegner, M.; Gerber, C.; Güntherodt, H.-J.; Lang, H. P. *Biosens. Bioelectron.* **2006**, *21*, 1599-1605.

16. Longo, G.; Alonso-Sarduy, L.; Marques Rio, L.; Bizzini, A.; Trampuz, A.; Notz, J.; Dietler G.; Kasas, S. *Nat. Nanotechnol.* **2013**, *8*, 522-526.

17. Zhang, J.; Lang, H. P.; Huber, F.; Bietsch, A.; Grange, W.; Certa, U.; McKendry, R.; Güntherodt, H.-J.; Hegner, M.; Gerber, C. *Nat. Nanotechnol.* **2006,** *1*, 214-220.

18. Huber, F.; Lang, H.P.; Backmann, N.; Rimoldi, D.; Gerber, C. *Nat. Nanotechnol.* **2013**, *8*, 125-129.

19. Braun, T.; Backmann, N.; Vögtli, M.; Bietsch, A.; Engel, A.; Lang, H. P.; Gerber, C.; Hegner, M. *Biophys. J.* **2006**, *90*, 2970-2977.

20. Barone, F.; Cellai, L.; Matzeu, M.; Mazzei F.; Pedone, F. *Biophys. Chem.* **2000** *86*, 37–47.

21. Benson, D. A.; Karsch-Mizrachi, I.; Lipman, D.J.; Ostell, J.; Sayers, E.W. *Nucl. Acids Res.* **2011**, *39* (suppl. 1), D32-D37.

22. Halait, H.; DeMartin, K.; Shah, S.; Soviero, S.; Langland, R.; Cheng, S.; Hillman, G.; Wu, L.; Lawrence, H. J. *Diagn. Mol. Pathol.* **2012**, *21*, 1-8.

23. Quintana, E.; Shackleton, M.; Foster, H. R.; Fullen, D. R.; Sabel, M. S.; Johnson, T. M.; Morrison, S. J. *Cancer Cell* **2010**, *18*, 510-523.

14

Supporting Information

Fast diagnostics of BRAF mutations in biopsies from malignant melanoma

François Huber*,†, Hans Peter Lang†, Katharina Glatz‡, Donata Rimoldi§, Ernst Meyer†,

Christoph Gerber*,†

† Swiss Nanoscience Institute, Department of Physics, University of Basel, CH-4056 Basel, Switzerland

‡ Institute of Pathology, University Hospital Basel, CH-4031 Basel, Switzerland

§ Ludwig Center for Cancer Research, University of Lausanne, CH-1066 Epalinges, Switzerland

*Corresponding authors: francois.huber@unibas.ch, christoph.gerber@unibas.ch

Methods
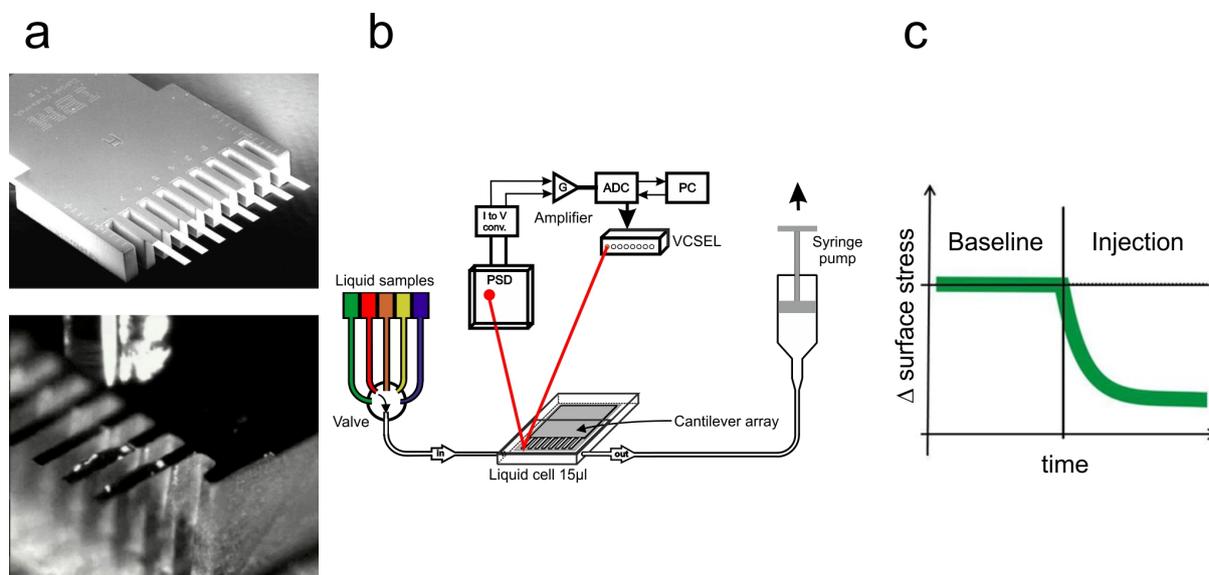
Figure S1. Experimental setup. (a) A microcantilever array (scanning electron microscope image shown above) is functionalized using an inkjet spotter and mounted into the liquid measurement chamber (volume of 15 μl). (b) Schematic drawing of the sensor instrument: Liquid cell with a mounted microcantilever array. Optical read-out system comprising of vertical cavity surface emitting lasers (VCSELs) and a position sensitive detector (PSD). Data acquisition and operation of the liquid handling system consisting of a multi valve selector, a syringe pump and temperature control are operated by a PC. The multi valve selector allows for different samples to be investigated and the syringe pump delivers liquids at 10 μl/min to the liquid measurement cell. A minimum of 500 ng sample can be used. (C) Progression of experiment; after equilibrating the system (baseline) with fresh 0.13 × SSC at 36 °C a sample is injected upon which a signal can be observed.

A microfabricated array of eight identical silicon cantilevers with a pitch of 250 μm, a length of 500 μm, a width of 100 μm, a thickness of 1 μm and a spring constant of 0.02 N/m were provided by the Micro-and Nanomechanics group at the IBM Research GmbH. The cantilever arrays were cleaned using an UV/Ozone cleaner (Jelight Company, Inc. Laguna Hills, California). Thiolated oligonucleotides (Microsynth AG, Balgach, Switzerland) were treated with 1 mM TCEP (Tris(2-carboxyethyl)phosphine, Sigma-Aldrich Chemie, Buchs, Switzerland) thereby reducing disulfide bonds to ensure efficient self-assembled monolayer formation. Functionalization was carried out at a concentration of 40 μM thiolated oligonucleotide in 50 mM TEAA buffer (triethyl ammonium acetate, Fluka, Buchs, Switzerland) using an MD-P-705-L inkjet dispensing system (Microdrop, Norderstedt, Germany). Afterwards the array was washed once with water and in buffer and mounted in the 15 μl volume measurement chamber. Samples were injected at 10 μl/min. Total RNA was extracted from tissue culture samples and biopsies using standard methods. The deflection signal in nm can be converted into a surface stress in mN/m using Stoney's equation and Sader's correction[1] with a Young's modulus of 1.2 x 10^{11} Pa for silicon, a cantilever thickness of 0.5 x 10^{-6} m and a Poisson ratio of 0.25.

RNA purification from cell cultures: Total RNA was extracted using Trizol reagent (In vitrogen) following manufacturer's instructions. RNA was further purified by ammonium acetate/ethanol precipitation and dissolved in DEPC-treated H_2O.

RNA purification from FFPE tissue: A 20 μm section was cut from each FFPE (formalin-fixed paraffin-embedded) block and collected in a tube. The sections were deparaffinized by two rinses in xylene. After paraffin solubilization, the tissue was rinsed twice in 100% ethanol and collected by centrifugation at 10,000 $\times$ g for 10 min. Alcohol was aspirated and the tissue pellets were resuspended in 480 μl of digestion buffer (Lysis buffer: 45 ml H_2O distilled + 5 ml 10X PCR

Buffer_AmpliGoldTaq + 50 μl ATL_Qiagen) and 20 μl of proteinase K (Promega 20 mg/ml) were added. Sections were incubated at 56°C overnight. Prior to RNA purification we inactivated proteinase K at 95°C for 10 min. Subsequently 1 ml of TRIzol® Reagent (Ambion Catalog number: 15596-026) was added per tube. The solution was vortexed and incubated at room temperature for 5 min. 1 μl of Glycogen (ThermoFisher Catalog number: R0551) was added to improve the RNA recovery, followed by 200 μL of BCP (Phase Separation Reagent MRC Catalog number: BP151). Each tube was vortexed vigorously for 30 sec and allowed to sit at room temperature for 3 min. Phase separation was achieved by centrifuging the sample at 12,000 × g for 15 min at 4°C. After centrifugation, the aqueous phase (containing the RNA) was carefully transferred to a new 1.5 ml Eppendorf Tube. The RNA from the aqueous phase was precipitated by mixing with 0.6 ml of isopropanol (99,9% pure) and stored at -20°C for 30 min. After that the sample was centrifuged at 12,000 × g for 30 min at 4°C. At this point the supernatant was removed and the RNA pellet was washed in 75% ethanol by vortexing. A final centrifugation step at 12,000 × g for 10 min at 4°C was performed. The ethanol was removed and the RNA pellet was briefly air-dried for 5 min. The RNA was re-suspended in 50 μl of RNase-free water (DEPC treatment) and incubated for 10 min at 60°C. RNA purity and concentration were determined by the absorbance at 260 nm (A260) and 280 nm (A280) using NanoDrop ND-2000 (Thermo Fisher Scientific, MA).

For experiments using total RNA from cell culture and melanoma tissue samples were diluted to 20 ng/μl in a 0.13 × SSC buffer equalling 20mM NaCl.

Table S1. List of oligonucleotides used for this work

Probe	Sequence	Experiment
BRAFV600E	5'-GAGATTTC**T**CTGTAGCTA-3'	Detection of BRAFV600E in total RNA
BRAFV600K	5'-GAGATTTC**TT**TGTAGCTA-3'	Distinguishing BRAFV600E from BRAFV600K
BRAFwildtype	5'-GAGATTTC**A**CTGTAGCTA-3'	Reference in BRAFV600E detection
polyAC	5'-ACACACACACACACACAC-3'	Reference for BRAF RNA detection
BRAFV600E complement	5'-TAGCTACAGA**G**AAATCTC-3'	Optimization of binding conditions
BRAFV600K complement	5'-TAGCTACA**AA**GAAATCTC-3'	BRAFV600K control experiment

Probe oligonucleotides and the corresponding experiments where they were used. The important bases for the detection are labelled in red.

Cantilevers were functionalized with corresponding 18mer probe thiol oligonucleotides (Table S1) and a 18mer reference oligonucleotide (polyAC). Initial experiments investigated optimal hybridization conditions and minimum concentrations for the detection of the mutation in total RNA extracted from biopsies. The most efficient hybridization temperature where only binding of *BRAF*^{V600E} mutant to the mutant BRAFV600E oligonucleotide occurs was evaluated (Figure S1). The experiments were based on theoretical estimates of the melting temperature and salt concentration for the BRAFV600E oligonucleotide (36.8 ±1.2 °C in 20mM NaCl). 36 °C and a saline sodium citrate (SSC) buffer containing 20mM NaCl turned out to be the most promising hybridization condition with the highest specificity. Whereas at 34 °C the *BRAF*^{V600E} signal is higher, we observe also a higher nonspecific wild type *BRAF* binding signal corresponding to

77% of the *BRAF^V600E* signal. No binding to the wild type reference by the mutated oligonucleotide is observed at 36 °C. At 38 °C the *BRAF^V600E* signal is diminished by 44% and at 40 °C is less than 10% of the signal at 36 °C. These studies suggest choosing 36 °C as the optimized temperature for the binding experiments.

Data analysis was done using OriginPro 2015 (OriginLab Corporation, Northampton, MA 01060, USA). Data were flattened using the locally weighted scatterplot smoothing (LOWESS) function and then a Langmuir function was fitted to the smoothed data. The dendrogram was computed using the hierarchical cluster analysis tool applying the Euclidian sum of distances method. The endpoints of the Langmuir fits right before the washing step with buffer were used for the creation of the dendrogram.
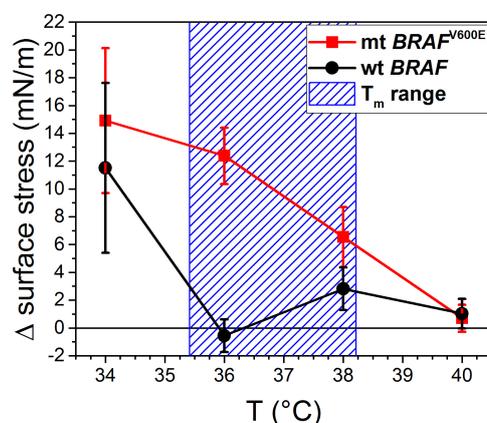
Figure S2. Temperature dependence of oligonucleotide binding: The red curve shows binding of the mutant oligonucleotide to the complement functionalized cantilever in dependence of the hybridization temperature whereas the black curve depicts binding of the wild type oligonucleotide to the cantilever functionalized with the mutated oligonucleotide. The blue

hatched area indicates the melting temperature (T_m) range. The results imply 36 °C as the most promising temperature for binding experiments.

REFERENCES

1. Sader, J. E. *J. Appl. Phys.* **2001**, *89*, 2911–2921.